ELSEVIER

Physica B 254 (1998) 178–187

PHYSICA B

Differential conductance of a saddle-point constriction with a time-modulated gate-voltage

C.S. Tang, C.S. Chu*

Department of Electrophysics, National Chiao Tung University, Hsinchu 30050, Taiwan

Received 24 March 1998; received in revised form 6 July 1998

Abstract

This work investigates how a time-modulated gate-voltage influences the differential conductance G of a saddle-point constriction. The constriction is modeled by a symmetric saddle-point potential and the time-modulated gate-voltage is represented by a potential of the form $V_0\,\Theta(a/2-|x-x_c|)\cos(\omega t)$. For $\hbar\omega$ less than half of the transverse subband energy level spacing, gate-voltage-assisted (suppressed) feature occurs when the chemical potential μ is less (greater) than but close to the threshold energy of a subband. Our results indicate that as μ increases, G exhibits, alternatively, the assisted and the suppressed feature. For a larger $\hbar\omega$, these two features may overlap. In addition, dip structures are found in the suppressed regime, and mini-steps are found in the assisted regime only when the gate-voltage covers a region sufficiently distant from the center of the constriction.

PACS: 72.10. − d; 72.40. + w

Keywords: Differential conductance; Quasi-bound-state; Quantum transport; Photocurrent

1. Introduction

The extent to which time-modulated fields influence the quantum transport has received extensive interest. These time-modulated fields can be transversely polarized [1–10], longitudinally polarized [11,12], or represented by time-modulated potentials, with no polarization [13–21]. The systems considered as of late are primarily mesoscopic systems, such as the narrow constrictions [1–10,17,21]. For a circumstance in which a constriction is acted upon by an incident electromagnetic wave, the time-modulated field has a polarization. Such a circumstance can be realized experimentally, as demonstrated by recent investigations [4,6]. On the other hand, the time-modulated potentials are expected to be realized in gate-voltage configurations [8,21], as depicted in Fig. 1.

The time-modulated fields, with or without polarizations, give rise to coherent inelastic scatterings. These inelastic scatterings do not conserve the longitudinal momentum along the transport direction, as long as the time-modulated fields have finite longitudinal ranges. This phenomenon is attributed to that the finiteness in the range of the fields breaks the translational invariance [9,21]. Furthermore, the inelastic scattering processes induced by these time-modulated fields depend also

* Corresponding author. Tel.: + 886 3 5712121.56127; fax: + 886 3 5725230; e-mail: cschu@cc.nctu.edu.tw.

0921-4526/98/$ – see front matter
PII: S0921-4526(98)00468-2

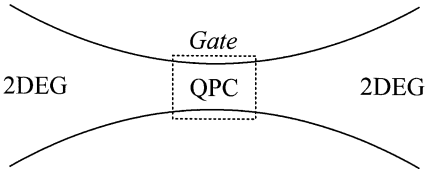

Fig. 1. Sketch of the gated saddle-point constriction which is connected at each end to a two-dimensional electron gas electrode. The gate induces a finite-range time-modulated potential in the constriction.

on the polarization of the fields. In an adiabatically varying constriction, the inelastic scattering processes involve inter-subband transitions when the time-modulated fields are transversely polarized. However, these processes involve only intra-subband transitions when the fields do not have polarizations, such as those arising from time-modulated gate-voltages. Hence, the detailed transport characteristics of the constriction depend on the polarization of the time-modulated fields.

In this work, we investigate how a time-modulated gate-voltage influences the differential conductance G of a saddle-point constriction. Of particular concern is the case of a time-modulated potential. The extent to which such a potential affects the transport properties of one-dimensional systems has received extensive attention [13–21]. However, the possible manifestation of quasi-bound-state (QBS) features has seldom been mentioned. An exception is Bagwell and Lake [17], who considered a time-dependent potential that has a delta profile. The energy of this QBS is below, but close to, the band bottom of a one-dimensional system. The transport exhibits QBS feature when the conducting electrons can make transitions via inelastic processes to the QBS. As expected, this QBS feature is more significant in a narrow constriction than in a one-dimensional system because there are, in a constriction, more subbands and hence more QBSs. Furthermore, the tunability of the subband structures and the chemical potential together provide a higher likelihood of probing the QBS feature in narrow constrictions.

Our earlier work [21] investigated the effect of a time-dependent gate potential acting upon the uniform-width region of a narrow constriction. According to those results, those electrons that manage to enter the narrow channel region from the two end-electrodes have perfect transmission. Consequently, the time-modulated potential cannot further increase the dc conductance. Instead, the potential causes backscattering, thereby lowering dc conductances. Hence, as expected, the dc conductance exhibits only gate-voltage-suppressed and not gate-voltage-assisted feature. As the chemical potential μ increases, dip structures at which μ is $m\hbar\omega$ above the threshold energy of a subband characterize the suppressed feature in the dc conductance. These dip structures are associated with the formation of QBS at a subband bottom in the narrow channel, as partially attributed to the singular density of states (DOS). Of relevant interest is whether such QBS feature persists in systems that have a large but not singular DOS. Cases that may have gate-voltage-assisted feature should also be explored.

In light of the above discussion, we examine a saddle-point constriction in a time-modulated gate-voltage. The following issues are addressed. First, the effective DOS in a saddle-point constriction is not singular, owing to that the singularity in the DOS of a narrow channel originates from the one-dimensionality and the sharp threshold energy of each subband. In a saddle-point constriction, the threshold energy of each subband is not sharp but is smeared by tunneling processes that occur near the threshold. Herein, the robustness of the QBS feature against the absence of a singular DOS is explored. Second, the gate-voltage encompasses regions in which the effective width of the constriction varies. The gate-voltage-assisted processes become feasible, which should be sensitive to the range of the gate-voltage. These range-dependent characteristics are studied herein. Third, the system can be easily configured into an asymmetric situation by shifting the center of the gate-voltage away from the symmetric center of the saddle-point constriction. The effect of this asymmetry is studied as well.

The rest of this paper is organized as follows. Section 2 presents the proposed method. Section 3 provides some numerical examples which demonstrate the proposed method's effectiveness. Concluding remarks are finally made in Section 4.

2. Theory

By selecting the energy unit $E^* = \hbar^2 k_F^2/2m^*$, the length unit $a^* = 1/k_F$, the time unit $t^* = \hbar/E^*$, and V_0 in units of E^*, the dimensionless Schrödinger equation for such saddle-point constriction becomes

$$\mathrm{i}\frac{\partial}{\partial t}\Psi(\boldsymbol{x},t) = [-\nabla^2 - \omega_x^2 x^2 + \omega_y^2 y^2 + V(x,t)]\,\Psi(\boldsymbol{x},t), \quad (1)$$

where k_F is a typical Fermi wave vector of the reservoir and m^* is the effective mass. The transverse energy levels $\varepsilon_n = (2n+1)\omega_y$ are quantized, with $\phi_n(y)$ being the corresponding wavefunctions. The time-modulated gate-voltage $V(x,t)$ can be expressed as

$$V(x,t) = V_0\ \Theta\left(\frac{a}{2} - |x - x_c|\right)\cos(\omega t), \quad (2)$$

where the interaction region is centered at x_c and with a longitudinal range a. Although the saddle-point constriction is symmetric, the transport characteristics could become asymmetric if the interaction region were not centered at the symmetric center of the constriction. On the other hand, the $V(x,t)$ considered herein is uniform in the transverse direction and it does not induce intersubband transitions. Thus, for a nth subband electron and with energy μ, incident along $\hat{x}$, the subband index n remains unchanged and the scattering wavefunction can be written in the form $\Psi_n^{(+)}(\boldsymbol{x},t) = \phi_n(y)\psi(x,t)$.

The wavefunction $\psi(x,t)$ can be expressed in terms of the unperturbed wavefunctions $\psi(x,\mu_n)$ which satisfy the Schrödinger equation

$$\left[-\frac{\partial^2}{\partial x^2} - \omega_x^2 x^2\right]\psi(x,\mu_n) = \mu_n\psi(x,\mu_n), \quad (3)$$

where $\mu_n = \mu - \varepsilon_n$ is the energy for the motion along $\hat{x}$. The solutions to Eq. (3) are doubly degenerate, given by [22]

$$\psi_e(x,\mu_n) = \exp\left(\frac{-\mathrm{i}\omega_x x^2}{2}\right)M\left(\frac{1}{4} + \mathrm{i}\frac{\mu_n}{4\omega_x}, \frac{1}{2}, \mathrm{i}\omega_x x^2\right), \quad (4)$$

$$\psi_o(x,\mu_n) = x\sqrt{\omega_x}\exp\left(\frac{-\mathrm{i}\omega_x x^2}{2}\right) \times M\left(\frac{3}{4} + \mathrm{i}\frac{\mu_n}{4\omega_x}, \frac{3}{2}, \mathrm{i}\omega_x x^2\right), \quad (5)$$

where ψ_e (ψ_o) denotes an even (odd) function of x, and $M(a,b,z)$ represents the Kummer's function [23]. For our scattering problem, it is more feasible to construct out of ψ_e and ψ_o wavefunctions that have the appropriate asymptotic behaviors. In the asymptotic region $x \to -\infty$, we construct wavefunctions ψ_{in} and ψ_{ref} which have only a positive and negative current, respectively. In the asymptotic region $x \to +\infty$, we construct wavefunction ψ_{tran} which has only a positive current. These wavefunctions are given by [22]

$$\psi_{in}(x,\mu_n) = \psi_o(x,\mu_n) + \alpha(\mu_n)\,\psi_e(x,\mu_n), \quad (6)$$

$$\psi_{ref}(x,\mu_n) = \psi_o(x,\mu_n) + \alpha(\mu_n)^*\,\psi_e(x,\mu_n), \quad (7)$$

$$\psi_{tran}(x,\mu_n) = \psi_o(x,\mu_n) - \alpha(\mu_n)^*\,\psi_e(x,\mu_n), \quad (8)$$

where

$$\alpha(\mu_n) = \frac{1}{4\pi}\left[\exp\left(\frac{-\pi\mu_n}{4\omega_x}\right) - \mathrm{i}\exp\left(\frac{\pi\mu_n}{4\omega_x}\right)\right] \times \left|\Gamma\left(\frac{1}{4} + \mathrm{i}\frac{\mu_n}{4\omega_x}\right)\right|^2, \quad (9)$$

and $\Gamma(z)$ is the Gamma function.

Using these wavefunctions allows us to write the wavefunction $\psi(x,t)$ for an electron incident from the left hand side of the constriction in the following form [14,21]:

$$\psi(x,t) = \psi_{in}(x,\mu_n)\mathrm{e}^{-\mathrm{i}\mu t} + \sum_m r_m^{(+)}(\mu_n, x_c) \times \psi_{ref}(x,\mu_n + m\omega)\mathrm{e}^{-\mathrm{i}(\mu+m\omega)t} \quad \text{if } x < x_0,$$

$$\psi(x,t) = \int \mathrm{d}\varepsilon[\tilde{A}(\varepsilon)\psi_{ref}(x,\varepsilon - \varepsilon_n) + \tilde{B}(\varepsilon)\psi_{tran}(x,\varepsilon - \varepsilon_n)]\,\mathrm{e}^{-\mathrm{i}\varepsilon t} \times \sum_p \left[J_p\left(\frac{V_0}{\omega}\right)\mathrm{e}^{-\mathrm{i}p\omega t}\right] \quad \text{if } x_0 < x < x_1,$$

$$\psi(x,t) = \sum_m t_m^{(+)}(\mu_n, x_c)\,\psi_{\mathrm{tran}}(x, \mu_n + m\omega) \times \mathrm{e}^{-\mathrm{i}(\mu+m\omega)t} \quad \text{if } x > x_1\,, \tag{10}$$

where n denotes the subband index, m represents the sideband index, and $J_p(x)$ is the Bessel function. The superscript $(+)$ in the transmission and the reflection coefficients indicates that the electron is incident from the left hand side of the constriction. In addition, the sideband index m corresponds to a net energy change of $m\hbar\omega$ for the outgoing electrons. The two ends of the interaction region are at $x_0 = x_c - a/2$ and $x_1 = x_c + a/2$.

The transmission and reflection coefficients can be obtained by matching the wavefunctions and their derivatives at the two ends of the time-modulated gate-voltage. For the matching to hold at all times, the integration variable ε in Eq. (10) must take on discrete values $\mu \pm m\omega$. Hence, $\tilde{A}(\varepsilon)$ and $\tilde{B}(\varepsilon)$ can be written in the following form:

$$\tilde{F}(\varepsilon) = \sum_m F(m)\,\delta(\varepsilon - \mu - m\omega)\,, \tag{11}$$

where $\tilde{F}(\varepsilon)$ refers to either $\tilde{A}(\varepsilon)$ or $\tilde{B}(\varepsilon)$. After performing the matching and eliminating the reflection coefficients $r_m^{(+)}(\mu_n, x_c)$, we obtain the equations relating $A(m)$, $B(m)$, and the transmission coefficients $t_m^{(+)}(\mu_n, x_c)$, as expressed in the following equations:

$$\begin{aligned}\psi_{\mathrm{tran}}(x_1, \mu_n + m\omega)\, t_m^{(+)}(\mu_n, x_c) &= \sum_{m'} [\, A(m')\,\psi_{\mathrm{ref}}(x_1, \mu_n + m'\omega) \\ &\quad + B(m')\,\psi_{\mathrm{tran}}(x_1, \mu_n + m'\omega)\,] \\ &\quad \times J_{m-m'}\left(\frac{V_0}{\omega}\right), \end{aligned} \tag{12}$$

$$\begin{aligned}\psi'_{\mathrm{tran}}(x_1, \mu_n + m\omega)\, t_m^{(+)}(\mu_n, x_c) &= \sum_{m'} [\, A(m')\,\psi'_{\mathrm{ref}}(x_1, \mu_n + m'\omega) \\ &\quad + B(m')\,\psi'_{\mathrm{tran}}(x_1, \mu_n + m'\omega)\,] \\ &\quad \times J_{m-m'}\left(\frac{V_0}{\omega}\right), \end{aligned} \tag{13}$$

and

$$\begin{aligned}&[\,\psi_{\mathrm{in}}(x_0, \mu_n)\,\psi'_{\mathrm{ref}}(x_0, \mu_n) - \psi'_{\mathrm{in}}(x_0, \mu_n)\,\psi_{\mathrm{ref}}(x_0, \mu_n)\,]\,\delta_{m0} \\ &\quad = \sum_{m'} [\,\psi_{\mathrm{ref}}(x_0, \mu_n + m'\omega)\,\psi'_{\mathrm{ref}}(x_0, \mu_n + m\omega) \\ &\qquad - \psi'_{\mathrm{ref}}(x_0, \mu_n + m'\omega)\,\psi_{\mathrm{ref}}(x_0, \mu_n + m\omega)\,] \\ &\qquad \times A(m')\,J_{m-m'}\left(\frac{V_0}{\omega}\right) \\ &\qquad + \sum_{m'} [\,\psi_{\mathrm{tran}}(x_0, \mu_n + m'\omega)\,\psi'_{\mathrm{ref}}(x_0, \mu_n + m\omega) \\ &\qquad - \psi'_{\mathrm{tran}}(x_0, \mu_n + m'\omega)\,\psi_{\mathrm{ref}}(x_0, \mu_n + m\omega)\,] \\ &\qquad \times B(m')\,J_{m-m'}\left(\frac{V_0}{\omega}\right), \end{aligned} \tag{14}$$

where $\psi' = \partial\psi/\partial x$.

By solving Eqs. (12)–(14), we obtain $t_m^{(+)}(\mu_n, x_c)$, $A(m)$, and $B(m)$, from which the reflection coefficients $r_m^{(+)}(\mu_n, x_c)$ can be calculated. The corresponding coefficients for electrons incident from the right-hand side of the constriction can be found by following a similar procedure. The validity of the transmission and the reflection coefficients can be checked by a conservation of current condition, given by

$$\sum_m \left| \frac{\Gamma\left(\frac{1}{4} + \mathrm{i}\frac{\mu_n + m\omega}{4\omega_x}\right)}{\Gamma\left(\frac{1}{4} + \mathrm{i}\frac{\mu_n}{4\omega_x}\right)} \right|^2 \exp\left(\frac{\pi m\omega}{4\omega_x}\right) \times [\,|t_m^{(\sigma)}(\mu_n, x_c)|^2 + |r_m^{(\sigma)}(\mu_n, x_c)|^2\,] = 1\,, \tag{15}$$

where superscript $\sigma = \pm$ denotes the direction of the incident particle. In our calculation, a sufficiently large cutoff to the sideband index is imposed. The $r_m^{(\sigma)}(\mu_n, x_c)$ and $t_m^{(\sigma)}(\mu_n, x_c)$ coefficients that we obtain are exact in the numerical sense.

The current transmission coefficient $T_{nm}^{\sigma}(E, x_c)$ is the ratio between the transmitting current in the mth sideband and the corresponding incident current due to a nth subband electron, with incident energy E and incident direction σ. This current transmission coefficient is related to the transmission

coefficient, as expressed in the following form:

$$T^{\sigma}_{nm}(E,x_c)=|t^{(\sigma)}_{m}(E_n,x_c)|^2\exp\left(\frac{\pi m\omega}{4\omega_x}\right)\times\left|\frac{\Gamma\left(\frac{1}{4}+i\frac{E_n+m\omega}{4\omega_x}\right)}{\Gamma\left(\frac{1}{4}+i\frac{E_n}{4\omega_x}\right)}\right|^2, \tag{16}$$

where $E_n=E-\varepsilon_n$. The total current transmission coefficient $T^{\sigma}(E,x_c)$ is defined as

$$T^{\sigma}(E,x_c)=\sum_n T^{\sigma}_n(E,x_c)=\sum_n\sum_m T^{\sigma}_{nm}(E,x_c). \tag{17}$$

Furthermore, in the case when the saddle-point potential is shifted by ΔU, the total current transmission coefficient becomes $T^{\sigma}(E-\Delta U,x_c)$.

According to our results, the total current transmission coefficients $T^{+}(E,x_c)$ and $T^{-}(E,x_c)$ are different for $x_c\neq 0$, when the interaction region is not centered at the symmetric center of the constriction. This difference can be understood from the following example. The entire interaction region is, for instance, on the right-hand side of the constriction and the incident energy E is chosen such that the electrons must tunnel through the constriction. In this example, an electron incident from the left hand side receives no assistance from the time-modulated gate-voltage when tunneling through the constriction. Instead, the electron suffers additional reflection from the gate-voltage after tunneling through the constriction. However, an electron incident from the right hand side can receive assistance from the gate-voltage while passing through the constriction. Of course, the electron might be reflected by this gate-voltage as well. However, in the opening up of a new gate-voltage-assisted transmission channel, the assisted feature dominates when the electron, after absorbing $m\hbar\omega$, can propagate (rather than tunnel) through the constriction. This example, although not a generic one, illustrates that the difference between the current transmission coefficients originates from the different extent to which the time-modulated gate-voltage is involved in assisting the transmitting electrons.

The fact that $T^{+}(E,x_c)$ can differ from $T^{-}(E,x_c)$ when a time-modulated potential acts upon the QPC leads to a nonzero current in an unbiased QPC. The current is the photocurrent I_{ph} (see below). Therefore, the transport in the QPC is more accurately represented by the differential conductance G, rather than the conductance or the total current transmission coefficient T.

To obtain the differential conductance in the low-bias regime, we choose the left reservoir as the source electrode such that the left reservoir has a chemical potential shift of $(1-\beta)\Delta\mu$, and the right reservoir has a chemical potential shift of $-\beta\Delta\mu$. In the low-bias regime, we have $\Delta\mu\ll\mu$. Martin-Moreno et al. [24] and Ouchterlony et al. [25] adopted the parameter β in their work on the nonlinear dc transport through a saddle-point constriction. The current I in the constriction can then be expressed by[1].

$$I=-\frac{2e}{h}\int_{-\infty}^{\infty}dE\,[f(E-\mu-(1-\beta)\Delta\mu)\,T^{+}(E,x_c)-f(E-\mu+\beta\Delta\mu)\,T^{-}(E,x_c)], \tag{18}$$

where $f(E)=[1+\exp(E/k_BT)]^{-1}$ is the Fermi function. In addition, $-e$ denotes the charge of an electron. By assuming that the lowest energy electrons from the reservoirs contribute negligibly to I, the lower energy limit of the above integral can be extended to $-\infty$. The zero temperature limit of Eq. (18) is given by

$$I=-\frac{2e}{h}\left[\int_{-\infty}^{\mu+(1-\beta)\Delta\mu}dE\,T^{+}(E,x_c)-\int_{-\infty}^{\mu-\beta\Delta\mu}dE\,T^{-}(E,x_c)\right]. \tag{19}$$

[1] One may want to use another current expression, which, in units of $-2e/h$, is given by

$$I=\int_{-\infty}^{\infty}dE\sum_{nm}\{f(E-\mu-(1-\beta)\Delta\mu)\times[1-f(E-\mu-m\omega+\beta\Delta\mu)]T^{+}_{nm}(E,x_c)-f(E-\mu+\beta\Delta\mu)[1-f(E-\mu-m\omega-(1-\beta)\Delta\mu)]\times T^{-}_{nm}(E,x_c)\}.$$

However, it can be shown that the two expressions give the same result.

The differential conductance in the low-bias regime, as defined by

$$G_0 = \left.\frac{\partial I}{\partial V_{sd}}\right|_{V_{sd}=0}, \tag{20}$$

can be calculated from differentiating Eq. (19), and is given by

$$G_0 = \frac{2e^2}{h}[\, T^+(\mu, x_c)(1-\beta) + T^-(\mu, x_c)\beta\,]. \tag{21}$$

Interestingly, G_0 depends on β whenever $T^+(\mu, x_c) \neq T^-(\mu, x_c)$. This β-dependence in G_0 does not occur for cases of purely elastic scatterings, such as impurity scatterings. We believe that G_0 is the major contribution to the differential conductance G. The other contribution to G is from the change in the photocurrent I_{ph} when the QPC is subjected to the low-biased transport field. This term is much smaller than G_0 and is qualitatively given by

$$G_{ph} = \frac{-e}{2\omega_x^2 L}\frac{\partial}{\partial x_c} I_{ph}(\mu, x_c), \tag{22}$$

where

$$I_{ph}(\mu, x_c) = -\frac{2e}{h}\int_{-\infty}^{\mu} dE[T^+(E, x_c) - T^-(E, x_c)] \tag{23}$$

is the photocurrent. Here L denotes the effective length of the potential drop across the QPC, and $\Delta\mu/(2\omega_x^2 L)$ represents the effective shift of the QPC position attributed to the small bias potential. The differential conductance $G = G_0 + G_{ph}$.

3. Numerical examples

In our numerical examples, the physical parameters are assumed to be in a high-mobility $GaAs - Al_xGa_{1-x}As$ heterostructure, with a typical electron density $n \sim 2.5 \times 10^{11}\,cm^{-2}$ and $m^* = 0.067 m_e$. Correspondingly, we choose an energy unit $E^* = \hbar^2 k_F^2/(2m^*) = 9\,meV$, a length unit $a^* = 1/k_F = 79.6\,\text{Å}$, and a frequency unit $\omega^* = E^*/\hbar = 13.6\,THz$. For the saddle-point constriction, we have chosen $\omega_x = 0.0125$, and $\omega_y = 0.05$ such that the effective length to width ratio of the constriction is $L_c/W_c = \omega_y/\omega_x = 4$. In presenting the dependence of G on μ, it is more convenient to plot G as a function of X, where

$$X = \frac{1}{2}\left[\frac{\mu}{\omega_y} + 1\right], \tag{24}$$

and the integral value of X denotes the number of propagating channels through the constriction.

To evaluate the term G_{ph} of the differential conductance G, the length L of the potential drop is assumed to be of the same order as L_c [26], where the length of our constriction $L_c = 4W_c = 8\sqrt{3/\omega_y} \simeq 62$ for a typical $n = 1$ subband. Following Ouchterlony et al.[2], who chose $L_c/L \approx 1.5$, we choose L to have a value $L = L_c/1.5 \simeq 41$.

Figs. 2–4 present the changes in the G characteristics when the range of the time-modulated potential is increased, from $a = 16$, 32, to 50, respectively. All these time-modulated potentials are centered, with $x_c = 0$, and have the same frequency ($\omega = 0.04$), and the same amplitude ($V_0 = 0.06$). The bias parameter $\beta = 0.5$ in these figures. The G characteristics are represented by the dependence of G on X, i.e., the appropriately rescaled chemical potential μ. According to this scale, a situation in which μ is changed by a subband energy spacing corresponds to $\Delta X = 1$. In addition, a situation in which μ is changed by $\hbar\omega$ corresponds to $\Delta X = \omega/(2\omega_y) = 0.4$. In addition, when $X = N$, μ is at the threshold of the Nth subband.

According to Fig. 2, both gate-voltage-assisted and gate-voltage-suppressed features are found in G. These two features occur in well separated regions of X. The gate-voltage-assisted regions occur when μ is merely beneath a subband threshold, and is most evident in the pinch-off ($X < 1$) region. Meanwhile, the gate-voltage-suppressed regions occur when μ is above but close to a subband

[2] In Ref. [25], Ouchterlony et al. have chosen the parameters: $m^* = 0.2m_e$, $\hbar\omega_y = 9\,meV$, and $\hbar\omega_x = 4.5\,meV$. Their length $L_c = 4\hbar\sqrt{3/(m^*\hbar\omega_y)} \simeq 11.3\,nm$ for a typical $n = 1$ subband. The length L over which the potential drop occurs was taken to be $L = 30\,nm$. Thus, in footnote 1, $L_c/L \approx 1.5$.

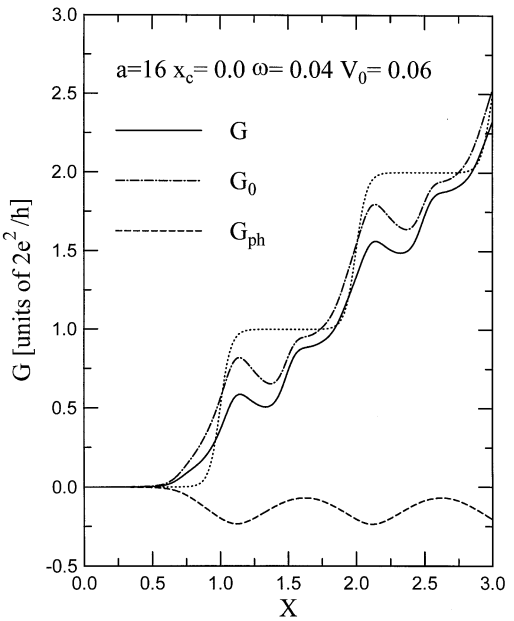

Fig. 2. Differential conductance G as a function of X for a centered time-modulated potential ($x_c = 0$), with oscillating amplitude $V_0 = 0.06$, frequency $\omega = 0.04$, and $\beta = 0.5$. The range of the potential $a = 16$ covers a distance up to $d = 8$ from the constriction center. The solid curve is the total differential conductance G, the dash-dotted curve is G_0, and the dashed curve is G_{ph}. In the assisted regime, although G_{ph} effectively suppresses the differential conductance, the general tunneling-like feature remains unchanged. In the suppressed regime, there are dip structures at $X = 1.4$ and 2.4.

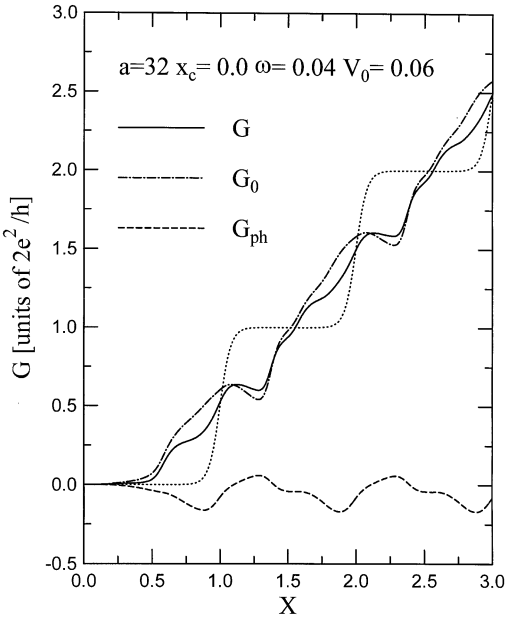

Fig. 3. Differential conductance G as a function of X for a centered time-modulated potential. The physical parameters are the same as in Fig. 3 except that the range of the potential is $a = 32$. The potential covers a distance up to $d = 16$ from the constriction center. In the assisted regime, the G_{ph} modifies the shoulder-like feature in G_0 and leads to the quasi-mini-step-like feature in G. In the suppressed regime, the dip structures at $X = 1.4$ and 2.4 are slightly modified by G_{ph}.

threshold. Dip structures are found in the suppressed region, at around $X = 1.4$ and 2.4, i.e., at $\Delta X = 0.4$ above a threshold. These dip structures are due to the processes that an electron in the Nth subband, and at energy $N + \Delta X$, can give away an energy $\hbar\omega$ and become trapped in the quasi-bound-state (QBS) immediately beneath the threshold [17,21]. In contrast with the QBS features in narrow channels [21], the QBS structures in a saddle-point contriction is much broader, indicating that the QBS life-time is much shorter due to the added possibility of escape via tunneling. In the gate-voltage-assisted region, G gradually increases, rather than abruptly, when a channel, after picking up an energy $\hbar\omega$, becomes propagating. This is because the range of the interacting region does not extend far enough so that the electron, although having the right energy, must tunnel to the interacting region first before being assisted. This also accounts for why no structures exist at $N \pm 2\Delta X$, which corresponds to the $2\hbar\omega$ processes. Consequently, the gate-voltage-assisted features do not affect the dip structures in the suppressed regions.

Notably, no harmonic feature could have been caused by the abrupt-profile of the the gate-voltage. This lack of such a feature is because the effective wavelength of a particle decreases as it emanates from the constriction so that multiple scattering between the two abrupt edges of the potential is subjected to rapid phase fluctuations, thereby suppressing any possible harmonic resonances. Thus, our results should also represent the cases of smooth-profile gate-voltages.

According to Fig. 3, the QBS structures at $X = 1.4$ and 2.4 are still evident. The assisted features are enhanced. In particular, in the pinch-off

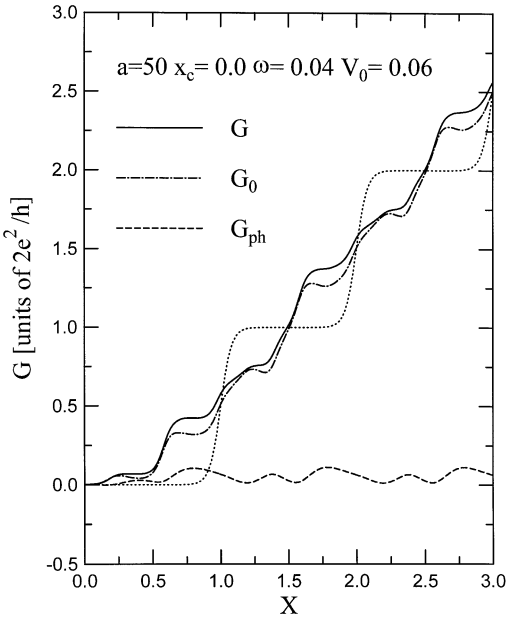

Fig. 4 . Differential conductance G as a function of X for a centered time-modulated potential. The physical parameters are the same as in Fig. 2 except that the range of the potential is $a = 50$, which covers a distance up to $d = 25$ from the constriction center. In the assisted regime, G_{ph} enhances G. Two mini-step-like structures are found in the pinch-off region.

region, G increases much faster, exhibiting a mini-step-like structure. The gate-voltage-assisted and the gate-voltage-suppressed features are well separated because no $2\hbar\omega$ features are found.

Fig. 4 reveals additional dip structures in G_0 at $X = 1.8$ and 2.8, indicating that $2\hbar\omega$ processes become significant. There are, of course, assisted features that involve one $\hbar\omega$ processes; they are the abrupt rises in G at $X = 0.6$, 1.6, and 2.6. The assisted feature that involves $2\hbar\omega$ is most apparent in the pinch-off region, around $X = 0.2$, where G exhibits another mini-step. Other 2ω assisted processes are at $X = 1.2$ and 2.2, which, unfortunately, are in the vicinity of the dip structures at $X = 1.4$ and 2.4. Hence, the dip structures become less dip-like but have turned into a sharp uplift in G because they are affected by the assisted features.

The assisted features in the above three figures differ from each other. Such a difference is related to how the electrons enter the interaction region. For the Nth subband electrons with incident energies that fall within the $m\hbar\omega$ interval below the threshold of the same subband, they are non-propagating. They can become propagating, and traverse through the constriction by absorbing $m\hbar\omega$ from the time-modulated potential. However, the electrons must be in the interaction region to absorb the needed energy. If the gate-voltage covers a region over a distance $d > d_m = \sqrt{m\omega}/\omega_x$ from the center, and on the incident side, of the constriction, the incident electrons can propagate into the interaction region. However, if the gate-voltage only covers regions over a shorter distance ($d < d_m$) from the constriction center, the electrons must tunnel into the interaction region. For $\omega_x = 0.0125$, we have $d_1 = 16$ and $d_2 \approx 23$. As mentioned earlier, the distances d covered by the gate-voltage are $d = 8$, 16, and 25, respectively, in Figs. 3, 4, and 5. Hence in Fig. 2, $d < d_1$, and the electrons must tunnel into the interaction regime so that the assisted feature, such as in the $X \leqslant 1$ region, exhibits a tunneling-like structure. According to Fig. 3, when $d = d_1$, the electrons can barely avoid entering the interaction region via tunneling, the assisted feature exhibits a quasi-mini-step-like structure. Fig. 4 indicates that when $d > d_2$, the electrons involved in the $2\hbar\omega$ processes can also propagate into the interaction region, and the assisted feature exhibits additional mini-step structures.

Fig. 5 presents the dependence of the G characteristics on the parameter β. The time-modulated gate-voltage is off-center, with $x_c = 3.0$, range $a = 32$, $V_0 = 0.06$, and frequency $\omega = 0.04$. The parameter $\beta = 0.2$, 0.5, and 0.8 in Figs. 5a–c, respectively. The curves in Fig. 5 indicate that G is quite sensitive to β. However, further analysis reveals that G_0, rather than G_{ph}, gives rise to the β-sensitivity in G. Hence, according to Eq. (21), as β increases, the contribution to G_0 from T^+ decreases while that from T^- increases. Since the assisted feature of T^- is more prominent than that of T^+ because $x_c = 3.0$. Therefore, the assisted features in the pinch-off region are progressively enhanced in Figs. 5a–c. This particular β-dependence simply reflects the asymmetry in $T^+(\mu, x_c)$ and $T^-(\mu, x_c)$, which occurs for coherent inelastic scatterings and not for elastic scatterings.

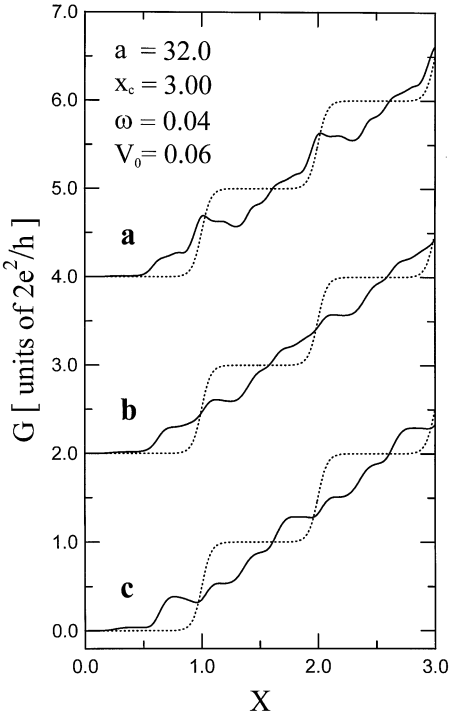

Fig. 5. Differential conductance G as a function of X for an off-centered time-modulated potential ($x_c = 3$), with range $a = 32$, frequency $\omega = 0.04$, and oscillating amplitude $V_0 = 0.06$. The parameter $\beta = 0.2$(a), 0.5(b), and 0.8 (c). The curves are vertically offset for clarity.

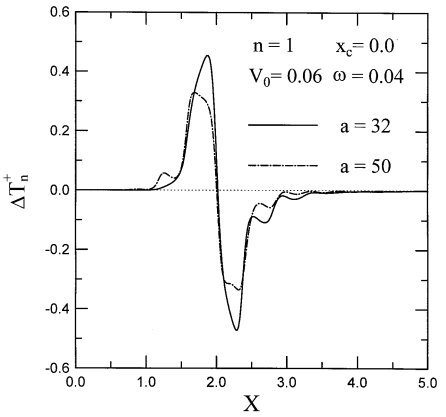

Fig. 6. ΔT_n^+ as a function of X for a centered time-modulated potential and subband $n = 1$, with frequency $\omega = 0.04$, $\beta = 0.5$, and oscillating amplitude $V_0 = 0.06$. The potential range $a = 32$ (solid) and 50 (dash-dotted). The assisted feature is found below $X = 2$ (the $n = 1$ subband edge), and the suppressed feature is found above $X = 2$. The $2\hbar\omega$ structures appear in the longer potential range ($a = 50$) case. The QBS features are at around $X = 2.4$, 2.8, and 3.2.

4. Conclusion

This study demonstrates that the differential conductance G, rather than the conductance or the current transmission coefficient, is the relevant physical quantity to characterize the low-bias transport, when a time-modulated field acts upon the QPC. This has not been recognised previously. Thus, comparing with the results of previous studies allows us to only turn to the current transmission coefficient. The deviation of the current transmission coefficient from its unperturbed value

$$\Delta T_n^+(E, x_c) = T_n^+(E, x_c) - \mathscr{T}_n^0(E),$$

was the photoconductance calculated by Grincwajg et al. [8], and Maaø et al. [10], when they considered a transverse electric field acting on a QPC with varying width. Here $\mathscr{T}_n^0(E) = 1/[1 + \exp(-\pi\varepsilon_n)]$, and n denotes the subband index of the incident electron. Fig. 6 plots our $\Delta T_n^+(E, x_c)$ results against X. The time-modulated potential is centered ($x_c = 0$), the frequency $\omega = 0.04$, the amplitude $V_0 = 0.06$, and the incident subband index $n = 1$. The threshold for the subband is $X = 2$. The assisted and the suppressed features are clearly shown below and above the threshold, respectively. This trend is the same as the results of Refs. [8,10], although the inelastic processes induced by a transverse field differs from that of a potential. On the other hand, our results have the added QBS features in the suppressed region, and the added 2ω feature in the assisted region for a longer potential range a. Both features are the major contributions of this study.

Finally, we have demonstrated the robustness of the QBS features. Whether these QBS features exist and remain robust in the cases of time-modulated electric field is currently under investigation.

Acknowledgements

The authors would like to thank the National Science Council of the Republic of China for

financially supporting this research under Contract No. NSC86-2112-M-009-004. Computational facilities supported by the National Center for High-performance Computing are gratefully acknowledged.

References

[1] F. Hekking, Y.V. Nazarov, Phys. Rev. B 44 (1991) 11506.
[2] Q. Hu, Appl. Phys. Lett. 62 (1993) 837.
[3] S. Feng, Q. Hu, Phys. Rev. B 48 (1993) 5354.
[4] R.A. Wyss, C.C. Eugster, J.A. del Alamo, Q. Hu, Appl. Phys. Lett. 63 (1993) 1522.
[5] L. Fedichkin, V. Ryzhii, V. V'yurkov, J. Phys. Condens. Matter 5 (1993) 6091.
[6] T.J.B.M. Janssen, J.C. Maan, J. Singleton, N.K. Patel, M. Pepper, J.E.F. Frost, D.A. Ritchie, G.A.C. Jones, J. Phys. Condens. Matter 6 (1994) L163.
[7] L.Y. Gorelik, A. Grincwajg, V.Z. Kleiner, R.I. Shekhter, M. Jonson, Phys. Rev. Lett. 73 (1994) 2260.
[8] A. Grincwajg, L.Y. Gorelik, V.Z. Kleiner, R.I. Shekhter, Phys. Rev. B 52 (1995) 12168.
[9] C.S. Chu, C.S. Tang, Solid State Commun. 97 (1996) 119.
[10] F.A. Maaø, L.Y. Gorelik, Phys. Rev. B 53 (1996) 15885.
[11] V.A. Chitta, C. Kutter, R.E.M. de Bekker, J.C. Maan, S.J. Hawksworth, J.M. Chamberlain, M. Henin, G. Hill, J. Phys.: Condens. Matter 6 (1994) 3945.
[12] M. Wagner, Phys. Rev. Lett. 76 (1996) 4010.
[13] M. Büttiker, R. Landauer, Phys. Rev. Lett. 49 (1982) 1739.
[14] D.D. Coon, H.C. Liu, J. Appl. Phys. 58 (1985) 2230.
[15] X.P. Jiang, J. Phys.: Condens. Matter 2 (1990) 6553.
[16] M.Y. Azbel, Phys. Rev. B 43 (1991) 6847.
[17] P.F. Bagwell, R.K. Lake, Phys. Rev. B 46 (1992) 15329.
[18] F. Rojas, E. Cota, J. Phys.: Condens. Matter 5 (1993) 5159.
[19] M. Wagner, Phys. Rev. B 49 (1994) 16544.
[20] O.A. Tkachenko, V.A. Tkachenko, D.G. Baksheyev, Phys. Rev. B 53 (1996) 4672.
[21] C.S. Tang, C.S. Chu, Phys. Rev. B 53 (1996) 4838.
[22] C.S. Chu, M.H. Chou, Phys. Rev. B 50 (1994) 14212.
[23] M. Abramowitz, I.A. Stegun, Handbook of Mathematical Functions, Dover, New York, 1972 p. 504.
[24] L. Martin-Moreno, J.T. Nicholls, N.K. Patel, M. Pepper, J. Phys.: Condens. Matter 4 (1992) 1323.
[25] T. Ouchterlony, K.-F. Berggren, Phys. Rev. B 52 (1995) 16329.
[26] I.B. Levinson, Zh. Eksp. Teor. Fiz. 95 (1989) 2175 [Sov. Phys. JETP 68 (1989) 1257].